Toward constraining regional-scale fluxes of CO_2 with atmospheric observations over a continent:
1. Observed spatial variability from airborne platforms

C. Gerbig,[1] J. C. Lin,[1] S. C. Wofsy,[1] B. C. Daube,[1,2] A. E. Andrews,[2] B. B. Stephens,[4] P. S. Bakwin,[5] and C. A. Grainger[6]

[1] We analyze the spatial variability of CO_2 measurements from aircraft platforms, including extensive observations acquired over North America during the CO_2 Budget and Rectification Airborne (COBRA) study in 2000. The COBRA data set is unique in its dense spatial coverage and extensive profiling in the lower atmosphere. Strong signatures of CO_2 fluxes at the land surface were observed in the active and relic mixed layers of the atmosphere (up to ~20 ppm gradients). Free tropospheric CO_2 exhibited significantly less variability except in areas affected by convective transport. Statistical analyses of the COBRA data indicate that CO_2 mixed-layer averages can be determined from vertical profiles with an accuracy of approximately ±0.2 ppm, limited by atmospheric variance. Analysis of the associated representation error suggests that models require horizontal resolution smaller than ~30 km to fully resolve spatial variations of atmospheric CO_2 in the boundary layer over the continent. To provide a global context for these data, we analyzed the GLOBALVIEW marine boundary layer (MBL) reference CO_2. Comparison of the MBL reference with extensive aircraft data extending over 20 years, covering the whole troposphere over the northern Pacific, shows significant seasonal biases of up to 2 ppm in the free troposphere, indicating that the MBL reference is a suitable boundary condition only for some applications. The spatial variability of CO_2 revealed by the COBRA-2000 calls for a suitable analysis framework to derive regional and continental fluxes, presented in a companion paper. The problem requires boundary conditions constrained by both surface and upper tropospheric observations and constraints on terrestrial fluxes that exploit the information content of the highly variable CO_2 distribution over land.   *INDEX TERMS:* 0315 Atmospheric Composition and Structure: Biosphere/atmosphere interactions; 0322 Atmospheric Composition and Structure: Constituent sources and sinks; 0368 Atmospheric Composition and Structure: Troposphere—constituent transport and chemistry; 1610 Global Change: Atmosphere (0315, 0325); 1615 Global Change: Biogeochemical processes (4805); *KEYWORDS:* regional carbon flux, spatial variability of CO_2

1. Introduction

[2] Projections of future atmospheric concentrations of CO_2 represent a major uncertainty in predicting future climate. A critical prerequisite for understanding the distribution of carbon sources and sinks over the globe and their responses to climate and environmental forcing is the capability to quantify regional- to continental-scale ($10^2 \sim 10^3$ km) sources/sinks on the basis of atmospheric data. Methods for quantifying the source/sink distribution will also be needed to verify mandated emission reductions and "carbon trading," should they come into effect.

[3] Atmospheric CO_2 measurements have played a key role in assessing source/sink distributions on global scales. Global emissions have been derived from long-term growth rates and inter-hemispheric differences [*Conway*

————————
[1]Department of Earth and Planetary Sciences and Division of Engineering and Applied Sciences, Harvard University, Cambridge, Massachusetts, USA.

[2]Now at Climate Monitoring and Diagnostic Laboratory, National Oceanic and Atmospheric Administration, Boulder, Colorado, USA.

[3]Now at NASA Goddard Space Flight Center, Greenbelt, Maryland, USA.

[4]Atmospheric Technology Division, National Center for Atmospheric Research, Boulder, Colorado, USA.

[5]Climate Monitoring and Diagnostic Laboratory, National Oceanic and Atmospheric Administration, Boulder, Colorado, USA.

[6]Department of Atmospheric Sciences, University of North Dakota, Grand Forks, North Dakota, USA.

et al., 1994] of atmospheric CO_2 concentrations, and more recently, continental/ocean basin-scale fluxes have been assessed using information contained in zonal gradients [e.g., *Fan et al.*, 1998]. A common method to infer sources and sinks from atmospheric measurements is to use a global tracer transport model to estimate the relationship between fluxes and tracer distributions, and then to derive source estimates using inverse techniques [e.g., *Bousquet et al.*, 1999; *Fan et al.*, 1998; *Tans et al.*, 1990].

[4] Estimates of continental CO_2 fluxes from inversion of global CO_2 measurements are affected by a variety of limitations: (1) Most inverse studies use data collected at stations remote from the terrestrial biosphere, situated to characterize global-scale gradients, and thus deliberately insensitive to regional-scale continental fluxes [*Gloor et al.*, 2000]; Monthly mean concentrations are usually used, intended to filter out "high-frequency variations" caused by weather systems, which are regarded as noise [*Gloor et al.*, 1999]. (2) Point measurements are not accurately represented in transport models that predict concentrations averaged over large grid cells. These spatial mismatches lead to "representation errors"; (3) Fluxes are aggregated over large regions to reduce the number of independent parameters, which may be problematic if the measurements used in the inversion are not evenly influenced by the whole region ("aggregation error") [*Kaminski et al.*, 2001]; (4) temporal covariances between mixed-layer height and biosphere-atmosphere exchange fluxes [*Denning et al.*, 1996] are usually not properly represented in models, causing biases over diurnal or seasonal timescales ("rectification errors"). New data analysis frameworks are required that address the above issues and that utilize the information contained in continental CO_2 measurements, such as made from aircraft and tall towers [e.g., *Bakwin et al.*, 1995, 1998; *Haszpra et al.*, 2001].

[5] Quantitative analysis of the characteristic spatial variability of CO_2 is a prerequisite to developing an appropriate framework to derive surface fluxes from atmospheric observations over the continent. First we must derive a boundary condition that reflects contributions to the measured CO_2 from outside the continent, in order to determine the CO_2 signal caused by continental sources and sinks. The variation of CO_2 with altitude and latitude over the Pacific determines the sophistication needed to derive this boundary condition. In particular, the capability of surface-based observations (where most measurements take place) in predicting values at higher altitudes needs to be assessed. Then we can assess the spatial variability of CO_2 over the continent associated with surface fluxes, the main factor controlling the error associated with the use of atmospheric observations in transport models.

[6] In this paper we determine the spatial variability of CO_2 in both the vertical and horizontal dimensions from data collected on the University of North Dakota Citation 2 aircraft during the CO_2 Budget and Rectification Airborne Study during August 2000 (COBRA-2000). The aircraft sampled extensively in both the vertical and the horizontal, covering spatial scales from a few km to hundreds and thousands of km. COBRA-2000 was designed as a pilot study to determine the characteristics of the atmospheric CO_2 signal from terrestrial ecosystem processes over North America and to test concepts to quantify sources and sinks

from those continental signals [*Stephens et al.*, 2000]. COBRA provides a snapshot of continental data that could be provided by future sampling networks with enhanced spatial coverage and multiple vertical profiles, allowing for the first time tests of data analysis frameworks proposed for the future. Data are compared with marine boundary layer reference values for CO_2 GLOBALVIEW [*GLOBALVIEW-CO2*, 2002] (also available on Internet via anonymous FTP to ftp.cmdl.noaa.gov, Path: ccg/co2/GLOBALVIEW) to put the COBRA data in the global context, and we assess the usefulness of the marine boundary layer reference CO_2 as a boundary condition for a regional modeling framework.

[7] Section 2 of this paper describes the measurements in COBRA-2000. In section 3 we present a statistical analysis of the COBRA data to examine the spatial variability in CO_2 and to derive the representation errors implicit in the observations; greater spatial heterogeneity means that an observation is representative only for a small region, with implications for design of observational systems [*Wofsy and Harriss*, 2002] and for the use of observations in inversion studies to quantify carbon sources/sinks. The COBRA data set with its dense spatial coverage provides an opportunity to derive for the first time a measurement-based representation error for scales between 10 and 100's of km. Variability in the vertical distribution determines the number of observations needed to characterize a vertical integral to specified precision, with consequences for flask sampling versus continuous sensors on airborne platforms [*Sarmiento and Wofsy*, 1999; *Tans et al.*, 1996].

2. Measurements in COBRA-2000

[8] Approximately 30 flight legs were conducted as part of COBRA over the United States and southern Canada during August 2000 with frequent vertical profiles from ~300 m to 10 km above ground, emphasizing the planetary boundary-layer (PBL). The University of North Dakota Cessna Citation-2 is a small, straight-wing twin-engine fan-jet, that can take off from relatively short airstrips and fly for significant distances in the PBL, at speeds as low as ~72 m/s (150 kts), but can also cover long distances (cruise at >150 m/s (300 kts)), and can profile as high as 12 km altitude.

[9] Measurements of CO_2 were made using a high-accuracy sensor flown previously on stratospheric balloons [*Daube et al.*, 2002], with a water trap added. In-flight calibrations were carried out every 20 minutes using standards traceable to the WMO Central CO_2 Laboratory [*Zhao et al.*, 1997] to an accuracy of 0.1ppm, and a measurement of the instrument null signal was done every 10 minutes. We obtained precision of ±0.25 ppm (2-σ) for the tropospheric measurements, somewhat poorer than achieved in the balloon configuration because of marginal performance of a solenoid valve. Data were recorded at 4 Hz and reported at 0.5 Hz, each datum representing the median of eight measurements.

[10] Measurements of CO were conducted using a modified commercial instrument (AL5001, Aero-Laser GmbH, Germany), based on the Vacuum-Ultraviolet (VUV) fluorescence technique, with a precision of 2 ppbv and a long-term accuracy of 3 ppb [*Gerbig et al.*, 1996, 1999]. Modifications included substituting the drier assembly as
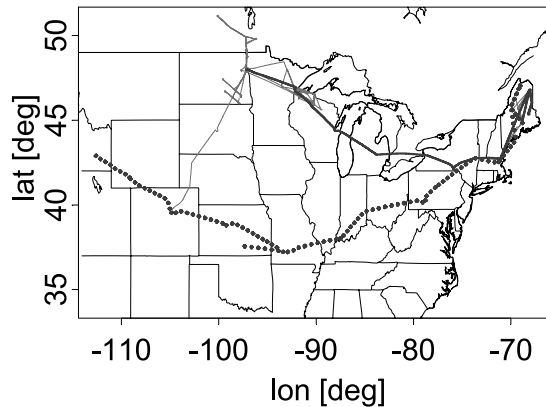
Figure 1. Flight routes of the Citation during the COBRA experiment in August 2000, comprising northern survey flights (dark gray solid line), southern survey flights (dark gray dotted line), and regional airmass following flights (light gray lines).

described by *Gerbig et al.* [1999], which improved stability of the zero signal significantly. The instrument sampled at 1 Hz and was automatically calibrated and zeroed at 30-minute intervals in flight using a standard gas mixture traceable to NOAA Climate Monitoring and Diagnostic Laboratory [*Novelli et al.*, 1992]. An identical VUV instrument showed excellent agreement with a tunable diode laser sensor in an airborne inter-comparison [*Holloway et al.*, 2000].

[11] Standard equipment was used for meteorological parameters: Dew point was measured with a cooled mirror hygrometer (EG&G, Model 137), temperature was observed using a Rosemount sensor (102 Probe), and static pressure was measured with a Rosemount transducer (1201F1).

[12] COBRA flights (Figure 1) were conducted on two spatial scales: (1) Regional ($\sim 10^4$ km^2) flights with multiple characterizations of the same airmass at different times were conducted to constrain fluxes at selected locations in North Dakota, Wisconsin (near the WLEF tall tower), and Maine, near the Howland Forest AmeriFlux site. These flights numbered 15, with about 100 vertical soundings covering $0.3 - 3$ km above ground level (AGL). (2) Trans-continental surveys (10 flight segments, Table 1) accounted for about 40 vertical profiles. This paper focuses primarily on CO$_2$ and CO measurements from the transcontinental surveys, except for the statistical analysis of representation error (section 2.2) that used the entire data set.

## 2.1. Observed Distributions of CO$_2$ and CO

[13] Two trans-continental surveys (Figure 1 and Table 1) covered the northern tier of the United States from Maine to North Dakota and the southern tier starting from Idaho and sweeping through Colorado, Kansas, the central Midwest, and north to Maine. The Citation cruised in the free troposphere, sounding the atmosphere vertically at 200-400 km intervals using "missed approaches" to small airports along the way. Vertical profiles were sampled at $\sim$600 m/min, giving a vertical resolution of $\sim$20 m for 2 second averages. This sampling strategy, combined with interpolation to facilitate interpretation of the numerous vertical profiles, generated cross sections showing distinct patterns due to surface fluxes at the continental scale (Figure 2).

[14] We observed a persistent deficit ($4 - 20$ ppm) of CO$_2$ in the lowest $2 - 3$ km of the atmosphere during the northern survey, a clear signature of CO$_2$ uptake by vegetation (Figure 2a). The smaller deficit around 84°W may indicate less uptake over the Great Lakes. However, there were slightly lower concentrations CO$_2$ in the free troposphere at

Table 1. Dates and Locations of Flights During COBRA2000[a]

Date (Start-End), GMT	Regions Flown Over (State)	Description	Number of Profiles Through PBL	stdev(CO$_2$), ppm
28 July, 20:38 – 22:42	ND, Ontario (CAN)	test flight	3	0.30
1 Aug., 12:10 – 14:47	ND, Ontario (CAN)	Lagrangian	NA	NA
1 Aug., 19:55 – 22:25	ND, Ontario (CAN)	Lagrangian	2	0.26
2 Aug., 13:05 – 15:22	ND	Lagrangian	16	0.78
2 Aug., 19:56 – 22:00	ND	Lagrangian	5	0.41
4 Aug., 15:40 – 17:59	ND, SD, NE, CO	survey	3	0.55
6 Aug., 14:35 – 16:07	ID, WY, CO	survey	3	0.44
6 Aug., 19:14 – 20:47	ID, WY, CO	southern survey	3	0.70
8 Aug., 14:31 – 16:38	CO, KS, MO	southern survey	2	0.48
9 Aug., 13:30 – 15:19	KS, MO, IL, IN	southern survey	4	0.58
9 Aug., 16:30 – 18:03	IN, OH, PA	southern survey	1	0.57
9 Aug., 18:52 – 20:25	PA, NY, MA	southern survey	2	0.72
11 Aug., 12:06 – 14:29	MA, NH, ME	Lagrangian/southern survey	2	0.44
11 Aug., 18:17 – 20:19	ME	Lagrangian	1	0.31
11 Aug., 21:42 – 22:26	ME, NH, MA	Lagrangian	1	1.06
18 Aug., 12:04 – 15:23	MA, NH, ME	Lagrangian	6	0.63
18 Aug., 18:19 – 20:53	ME, NH, MA	Lagrangian/northern survey	4	0.42
19 Aug., 12:17 – 14:42	MA, NH, VT, NY, Ontario (CAN), MI	northern survey	3	0.90
19 Aug., 15:28 – 16:28	MI, WI	northern survey	2	1.34
19 Aug., 17:58 – 19:50	WI, MN, ND	northern survey	4	0.71
23 Aug., 12:39 – 15:21	ND, WI, MN	Lagrangian	5	0.99
23 Aug., 17:34 – 19:11	WI, MN	Lagrangian	4	0.63
23 Aug., 21:04 – 23:18	WI, MN, ND	Lagrangian	11	0.41
24 Aug., 12:31 – 14:37	ND, WI, MN	Lagrangian	5	0.62
24 Aug., 17:37 – 18:55	WI, MN	Lagrangian	4	0.45
24 Aug., 21:04 – 23:18	WI, MN, ND	Lagrangian	7	0.44

[a]Here, stdev(CO$_2$) refers to the standard deviation within the mixed layer, averaged over the profiles with substantial vertical coverage throughout the mixed layer.
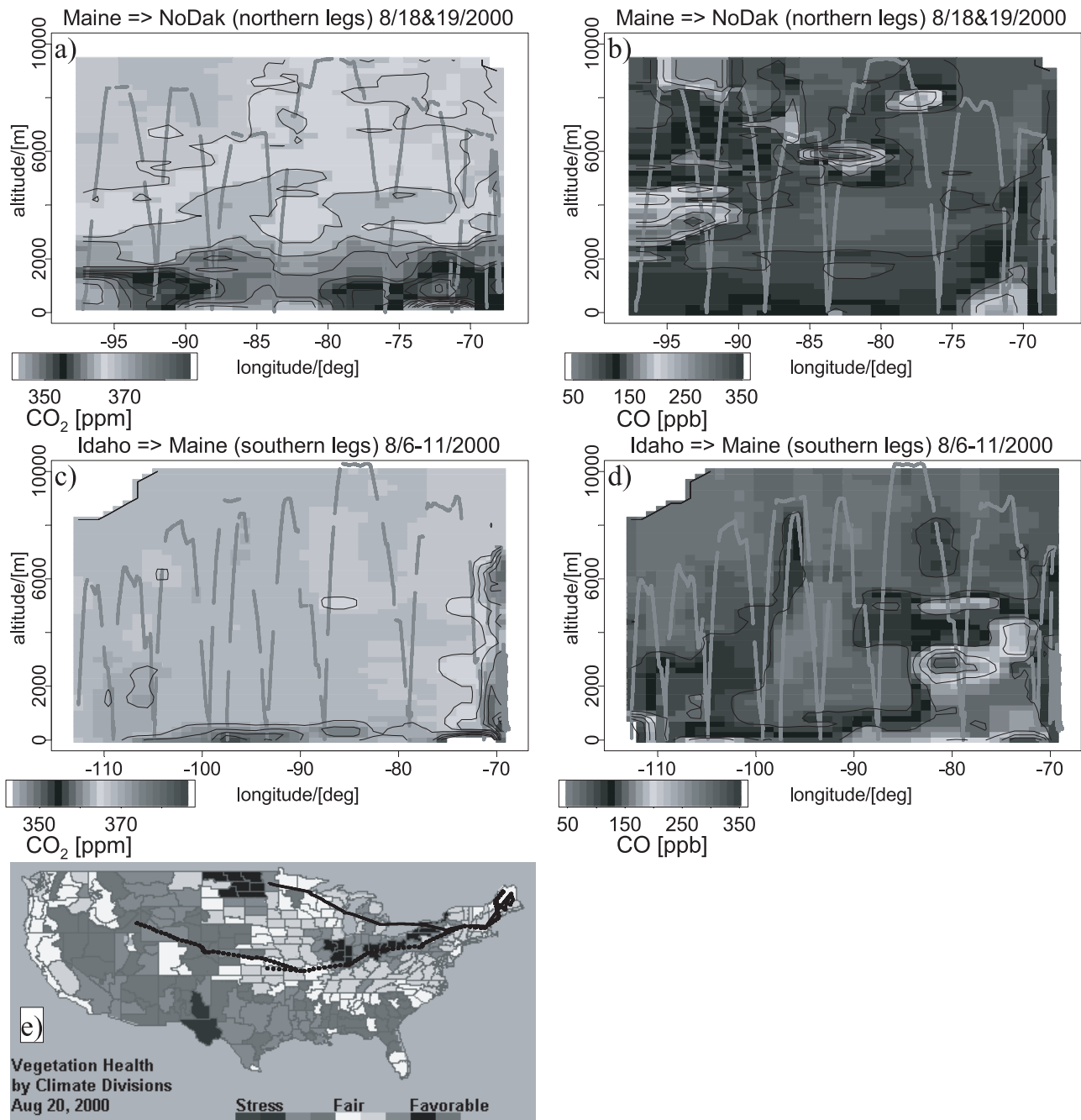
Figure 2. Measured CO_2 and CO distribution as a function of altitude and longitude for the (a and b) northern and (c and d) southern transects, and (e) vegetation condition index (from NESDIS) for 20 August 2000; approximate flight tracks are superimposed. To interpolate the tracer data in altitude and longitude between the measurement locations, the squared inverse of the distance was used as weighting, with the distance measured in units of 500 m vertical and degree longitude horizontal (aspect ratio 1/200). Tracer data from different days and different times of the day are represented in the cross sections (see Table 1). See color version of this figure at back of this issue.

the same location compared to further east or west, which could also point to convective activity, causing mixed-layer air lower in CO_2 to be vented upward and replaced in part by free tropospheric air with higher CO_2. Enhanced CO_2 was measured during the morning take off over Massachusetts, at 71°W, because of both local emissions of fossil fuel CO_2 and night time respiration from vegetation into the shallow mixed layer. Otherwise we sampled mostly the

residual mixed layer from the previous afternoon in the eastern part of the transect, and the deep afternoon mixed layer in the western part, and thus we did not observe much influence from nocturnal respiration in the shallow mixed layer in the early part of the day.

[15] We observed enhancements of CO_2 exceeding 10 ppm in the lowest part of the atmosphere on the southern survey (Figure 2c), in marked contrast to the northern
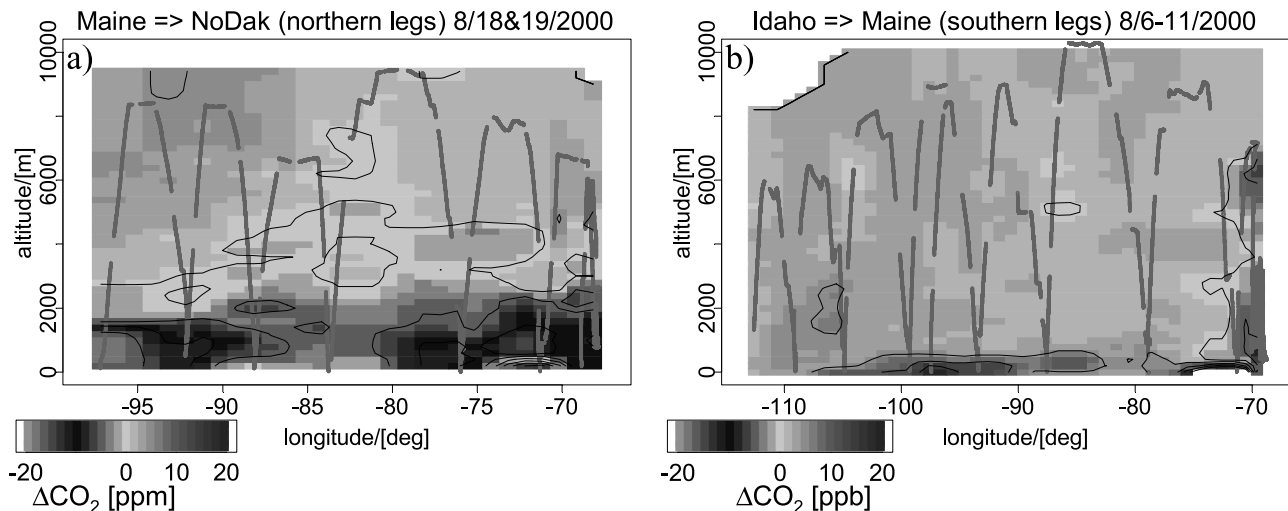
Figure 3. Difference of measured CO$_2$ and MBL-reference CO$_2$ as a function of altitude and longitude for the (a) northern and (b) southern transects. Interpolations are done similar to those in Figure 2. See color version of this figure at back of this issue.

survey. These regions of the west and southeast were affected by strong seasonal drought, as indicated by the vegetation condition index for 20 August 2000 (Figure 2e). This index, provided by the National Environmental Satellite, Data, and Information Service (NESDIS) http://orbit-net.nesdis.noaa.gov/crad/sat/surf/vci/uscd/usacd.html) and based on AVHRR radiance data, provides a measure of vegetation stress [*Kogan*, 1997]. During the southern survey, conditions were also cloudy in much of the region just upwind of the flights, further limiting photosynthesis. The unfavorable growing conditions, cloudiness, and emissions of CO$_2$ from fossil fuel combustion led to enhancements of CO$_2$ across the whole southern part. Over Maine, at the end of the transect, CO$_2$ was depleted by about 10 ppm in the lowest 2 km, but also by the same amount in the free troposphere at around 6 km. This was a clear signature of convective activity that vertically redistributed air with low CO$_2$ concentrations from the mixed layer into the middle troposphere.

[16] The distribution of CO (Figures 2b and 2d) exhibits notable layering with enhanced mixing ratios in the middle troposphere, caused by emissions from extensive fires in Idaho and Colorado. Mixing ratios of CO exceeding 300 ppb were found both in free tropospheric haze layers along the survey flights and in the mixed layer of the westernmost profile of the southern survey, close to the sources. The enhanced CO in the mid troposphere coincides with aerosol layers observed by the TOMS satellite (available from http://toms.gsfc.nasa.gov/aerosols/aerosols.html). CO from anthropogenic emissions was seen during take-off and landing near Boston, 71°W, and Denver, 105°W.

2.2. Comparison With Background CO$_2$

[17] An estimate of the CO$_2$ signal caused by continental sources and sinks (biospheric and combustion processes) can be derived by subtracting from the observed CO$_2$ distributions a CO$_2$ background, which accounts for contributions to the measured CO$_2$ advected from outside the continent. Here we used the marine boundary layer refer-

ence (MBL- reference) CO$_2$ provided by the GLOBAL-VIEW data set [*Masarie and Tans*, 1995; *GLOBALVIEW-CO$_2$*, 2002]. The MBL-reference data set combines marine station data of CO$_2$ into a consistent function of time and latitude.

[18] Differences between COBRA CO$_2$ and the MBL-reference CO$_2$ taken at the same time and latitude (Figure 3) reveal the strong continental signals, with large variability of up to 20 ppm confined mostly to the mixed and residual layer. Concentrations of CO$_2$ in the free troposphere (above 3 km) are 0–2 and 1–3 ppm above the MBL-reference for the northern and southern survey, respectively, and show significantly less variability than at lower altitudes, with the exception of the convective signature in the easternmost part of the southern survey (over Maine). These results suggest that atmospheric CO$_2$ in the free troposphere is largely determined by concentrations in the marine boundary layer upstream; most of the information about surface fluxes resides in the continental PBL. The rough separation of influences on the vertical distribution provides the basis for interpreting the depletions and enhancements in CO$_2$ shown in Figure 3 in terms of a modeling framework to derive fluxes from biospheric and combustion processes.

3. Statistical Analysis of Spatial Variance and Covariance

[19] The spatial scales of variance and covariance for atmospheric mixing ratios represent a critical factor for the resolution of a transport model linking local tracer mixing ratios to tracer fluxes upstream. The distinct CO$_2$ signals caused by surface fluxes are mainly confined to the lower troposphere, particularly the mixed layer and the residual layer (Figure 3). COBRA observations provide a first impression to characterize the statistical properties of the associated changes in CO$_2$. Transport models cannot represent the particulars of small-scale filaments that we observed within the mixed layer, which are caused by turbulent eddies (air entrained from the free troposphere and plumes
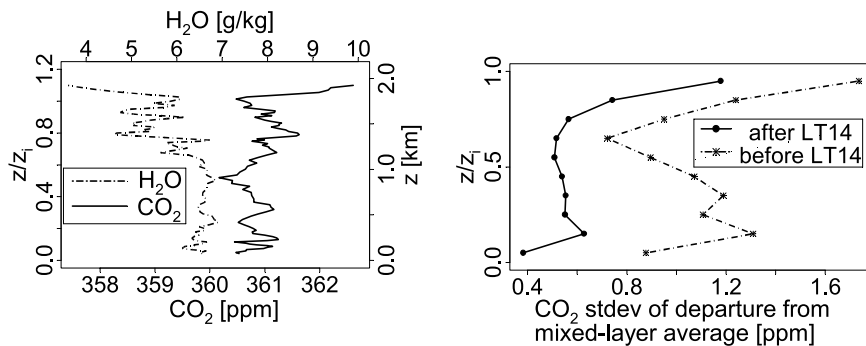
Figure 4. Profiles of CO$_2$ and H$_2$O collected around 15:00 local time over Duluth, MN (left). Profiles of the standard deviation of the departure from the mixed-layer average CO$_2$ (right). Afternoon values are less variable (solid circles and solid lines) than morning/noon values (stars and dashed line). A distinct increase in variability at the upper 20% of the mixed layer is due to intermittent entrainment of air from the residual layer or free troposphere.

caused by rising thermals from the surface). Hence the mean value of tracer concentration averaged over the mixed layer should be the quantity compared between models and observations.

[20] In the following sections, we analyze intrinsic sampling error, the accuracy of mixed-layer averages determined from in situ profiles, as well as the representation error, the uncertainty introduced when the mixed-layer averages at a point are represented in transport models with finite grids (related to the "grain-size" of the spatial distribution of CO$_2$). The sampling error includes both limitations in instrument precision and accuracy and uncertainty of the mixed-layer averages caused by unresolved atmospheric variability of CO$_2$ within the mixed layer due to turbulent eddies (see Figure 4, left).

3.1. Uncertainty of Mixed-Layer Averages From Individual Profiles

[21] To calculate mix-layer averaged mixing ratios, the mixed-layer height z_i was first determined from observed tracer profiles as the altitude at which the vertical gradient of potential temperature, $d\theta/dz$, increases, as well as where step changes in H$_2$O, CO$_2$ and CO are found. The average CO$_2$ concentration in the mixed layer, $\overline{CO_2}$, was then calculated for the over 100 profiles collected during COBRA as the mass weighted average, excluding the top 20% of the mixed layer to avoid the most active entrainment zone as well as ambiguities as to the top of the mixing zone. The standard deviation of individual measurements in the mixed layer (Figure 4, right) was derived by calculating the standard deviation about the mean for the whole profile in a given altitude bin over all profiles. The mean standard deviation for the 100 profiles was ~0.6 ppm for the afternoon (>14:00 local time) and ~1 ppm for morning profiles (<14:00 local time). Atmospheric variability within the mixed layer dominated the variance associated with the precision of the CO$_2$ measurements (1-σ ~ 0.13 ppm).

[22] The variance of $\overline{CO_2}$ cannot be calculated by simply dividing the square of the standard deviation by the number of observations, since observations are spatially correlated because of the presence of tracer layers (Figure 4, left). Instead, we can use the following approach [after *Wei*, 1989,

p. 18] to calculate the variance of $\overline{CO_2}$, then uncertainty in $\overline{CO_2}$ are related to the square root of this variance:

$$\sigma^2\left(\overline{CO_2}\right) = Var\left(\overline{CO_2}\right) = Var\left(\frac{1}{n}\sum_{j=1}^{n} CO_2(z_j)\right)$$

$$= \frac{1}{n^2}\sum_{j=1}^{n}\sum_{k=1}^{n} Cov\left(CO_2(z_j), CO_2(z_k)\right)$$

$$= \frac{1}{n}\sum_{l=-(n-1)}^{n-1}\left(1 - \frac{|l|}{n}\right) \cdot \mu_l \text{ with } l = j - k \qquad (1)$$

[23] Here the profiles were regridded into altitude bins (j, k) of 20 m vertical, *Var* and *Cov* stand for variance and covariance, respectively, and μ_l denotes the autocovariance function at lag l. For simplicity the mass weighting used to calculate $\overline{CO_2}$ was neglected in assessing errors. Sampling error values range from 0.02 to 0.9 ppm for individual profiles, with a mean over all profiles of 0.19 ppm (0.13 ppm for afternoon profiles only, and 0.22 ppm for morning profiles only). Geographic differences in the sampling error could not be identified even though mixed-layer profiles from many different areas were included in the analysis (see Figure 1 and also Table 1).

3.2. Spatial Correlation of Mixed-Layer Averages

[24] The geostatistical method of variogram estimation was employed to assess the spatial variability of the mixed-layer averaged CO$_2$ (in the following referred to as signal S), and to derive measurement-based estimates for the representation error for given spatial resolutions in transport models. The variogram is the variance of the difference of signals (var($S_i - S_j$)) measured at different locations x_i, x_j, as a function of distance $|x_i - x_j|$ between the points of measurement [*Cressie*, 1993]. In order to minimize the influence of temporal variation on S, we used only pairs of observations that were obtained within three hours of each other. The estimated variogram is then used to simulate many of possible realizations of the spatial distribution for S that follow the observed spatial variation and are consistent with a particular point measurement, allowing us to estimate the uncertainty in comparing the grid average computed by a transport model with local point measurements, i.e., the
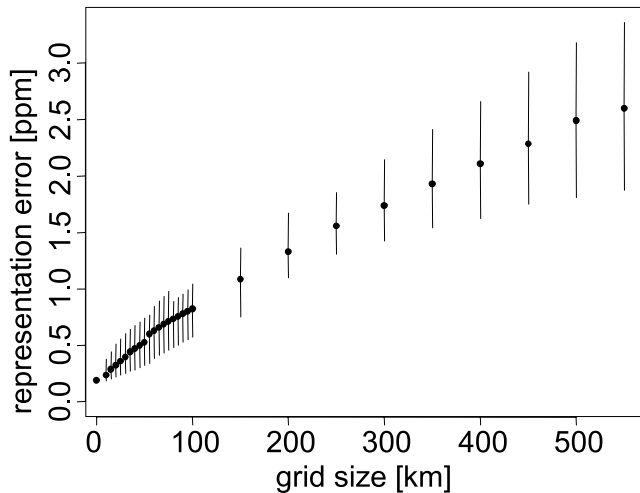
Figure 5. Total representation error of mixed-layer averaged CO$_2$ mixing ratios (combined sampling error and representation error) plotted against the horizontal dimension of the region. Vertical bars indicate the 5–95% confidence intervals.

representation error. Details of the statistical treatment are presented in Appendix A.

[25] Since the statistical analysis included the variance due to the sampling error, the calculated uncertainty includes both the representation error and the sampling error in COBRA-2000. Therefore in the following we refer to this combined error as the total representation error, a measure of the overall uncertainty associated with using a mixed-layer averaged CO$_2$ from a local profile measurement to represent a larger region. The results presented in Figure 5 show a significant increase of the total representation error with horizontal grid size. The analysis also provided an estimate of the uncertainty in the calculated error, expressed in the range for the central 90% (indicated by the vertical bars in Figure 5). The effect of the sampling error is evident at very small grid sizes, where the representation error is small, i.e., total representation error approaches the sampling error at zero grid size. Representation error starts dominating the sampling error in the total representation error at ~30 km, where true representation error is twice as large as the sampling error; at a grid size of ~100 km total representation has increased to 0.8 ppm. We note that these values strictly apply for the COBRA flights, and might be different at other locations or times.

4. Discussion

4.1. CO$_2$ Signal From Continental Fluxes

[26] It would be tempting to interpret observed differences between continental concentrations and the MBL reference, presented in Figure 3, as signatures due to fluxes over North America. However, the assumption that the background field depends solely on the time and latitude of the measurement is unlikely to be correct in general. Vertical gradients are almost certainly present upwind of the continent, and the remote areas influencing a particular measurement are typically not at the same latitude as the

observation. Both issues could can cause biases in the signal, and therefore need serious attention. The presence of vertical gradients is addressed below by comparisons to data from airborne and surface measurements over the Pacific; the meridional transport of CO$_2$ between remote marine locations and mid-continental sites will be addressed in the companion paper [*Gerbig et al.*, 2003], in which we couple a lateral boundary condition to a transport model to derive background contributions to the observed concentrations.

[27] To investigate the potential of bias associated with assuming constant concentration in the vertical over the Pacific, we compared the MBL reference to extensive data for CO$_2$ made from surface stations and aircraft (Table 2). The data set combines measurements of CO$_2$ collected above 300 m (see Table 2), between the Pacific coast and 180°W (north of 70°N, the longitude range was gradually relaxed, so that at 90°N all longitudes where used). We also included data collected in flasks above 5 km at Carr, Colorado. Of the flask data collected at ground sites only samples representative for background conditions were used. Aircraft data with potential influence from the stratosphere were excluded using a filter based on O$_3$, N$_2$O, CO, potential temperature, H$_2$O, and altitude.

[28] For each measurement in this data set we calculated the difference between the measured CO$_2$ and MBL-reference CO$_2$ taken at the same time and latitude. Figure 6 shows the mean distribution of residuals (measurements − MBL-ref.) for 2 km altitude bands for each month, representing the mean vertical gradient of CO$_2$ over the Pacific. These gradients are associated with the vertical propagation of seasonal changes in the global net surface flux, and evidently would lead to bias if the MBL-reference for CO$_2$ were assumed to represent the boundary condition for mid-tropospheric air at all altitudes over North America. Significant bias of up to 3 ppm (MBL-ref. lower than measurements) is observed at altitudes above 2 km in winter and spring, while during the summer a 2 ppm bias of opposite sign is found. For the COBRA period in August 2000, this artifact partly accounts for the positive values of the difference CO$_2$(COBRA) − CO$_2$(MBLref) in the free troposphere (Figure 3). At lower altitudes, no significant bias was found, even though the MBL-reference is constructed from oceanic stations around the globe rather than just Pacific stations, because differences are small between the Atlantic and the Pacific (~0.3 ppm [*Fan et al.*, 1998]).

[29] The monthly profiles of the residuals in Figure 6 are clearly related to vertical propagation of seasonal changes in surface flux. The phase of the seasonal cycle is delayed and the amplitude declines with altitude [cf. *Nakazawa et al.*, 1991]. Hence CO$_2$ can be interpreted as a tracer for the age of air in the troposphere since contact with the surface, equivalent to using stratospheric CO$_2$ to determine the age of air since entry into the stratosphere [*Andrews et al.*, 1999]. During the summer months (August–September), for example, surface CO$_2$ is decreasing rapidly, while the upper and middle atmospheric CO$_2$ lag behind by 1 to 2 months, respectively. The summertime residuals are actually largest in the middle troposphere, likely related to convective pumping of air to the upper troposphere, leaving the "oldest" air in the middle troposphere.

Table 2. Data Used in the Climatology for the Boundary Condition (CO and CO_2), Together With Corresponding Time Periods, Locations, and Data Source[a]

Campaign/Platform	Date (Start-End)	Latitude, °N	Longitude, °W	Altitude, km	Source
Barrow (BRW)	1980–2002	71	156	0	CMDL
Cold Bay (CBA)	1980–2002	55	162	0	CMDL
Cape Kumukahi (KUM)	1980–2002	20	154	0	CMDL
Mauna Loa (MLO)	1980–2002	20	155	3	CMDL
Molokai, HI (HAA)	31 May 1999 to 14 May 2001	20	155	0–8	CMDL
Poker Flats, AK (PFA)	27 June 1999 to 30 Nov. 2002	20	155	1–7	CMDL
Commercial B747	1 Jan. 1984 to 8 Dec. 1985	20–61	149–220	7–11	*Nakazawa et al.* [1991]
PEM-West-A (DC8)	18 Oct. 1991 to 21 Oct. 1991	16–34	136–180	0–12	GTE
AASE-2	14 Jan. 1992 to 13 March 1992	10–90	27–347	1–12	ESPO
PEM-West-B (DC8)	8 Feb. 1994 to 14 March 1994	21–61	122–180	0–10	GTE
ASHOE/MAESA	18 March 1994 to 29 Oct. 1994	20–22	157–159	9–13	ESPO
ACE-1	31 Oct. 1995 to 23 Dec. 1995	10–76	123–160	0–8	CODIAC
TOTE/VOTE	8 Dec. 1995 to 19 Feb. 1996	10–82	119–180	1–13	ESPO
SUCCESS	11 May 1996 to 14 May 1996	38–46	123–127	3–12	ESPO
PEM-Tropics A (P3)	18 Aug. 1996 to 31 Aug. 1996	10–37	123–165	0–8	GTE
PEM-Tropics A (DC8)	30 Aug. 1996 to 6 Oct. 1996	10–45	123–158	0–10	GTE
STRAT	26 Oct. 1995 to 12 Dec. 1996	20–37	121–161	9–13	ESPO
Carr (CO)	17 July 1995 to 1 Jan. 1997	41–41	105–105	5–8	CMDL
POLARIS	26 June 1997 to 23 Sept. 1997	20–66	145–159	0–12	ESPO
PEM-Tropics B (P3)	11 March 1999 to 9 April 1999	10–33	119–158	0–7	GTE
PEM-Tropics B (DC8)	6 March 1999 to 18 April 1999	10–33	105–164	0–12	GTE
Trace-P (DC8)	26 Feb. 2001 to 9 April 2001	18–40	120–180	0–11	GTE
Trace-P (P3)	26 Feb. 2001 to 9 April 2001	16–34	120–180	0–8	GTE

[a]Acronyms for data sources are as follows: CMDL, NOAA Climate Monitoring and Diagnostics Laboratory, Carbon Cycle Group (Cooperative Air Sampling Network); GTE, Global Tropospheric Experiment, from NASA Langley Research Center Atmospheric Sciences Data Center http://cloud1.arc.nasa.gov/index.html); ESPO, NASA Ames Research Center Earth Science Projects Office Missions http://esposarchive.nasa.gov/archive/); CODIAC, Joint Office for Science Support (JOSS) UCAR Data Management Center http://www.joss.ucar.edu/codiac/).

[30] The seasonally dependent vertical gradient for CO_2 over the ocean can lead to significant systematic errors in assessing the magnitude of concentration changes attributed to continental surface fluxes. These errors might be greater than expected where large-scale subsidence advects air from the free troposphere upstream of the continent to altitudes near the continental surface, where the signals of terrestrial carbon fluxes are the strongest. In the companion paper we use the extensive data set of CO_2 at altitude to generate a boundary condition with significantly reduced seasonal bias, accounting for the altitude-dependence through a Green's function that relates time-dependent concentrations of CO_2 at the surface to those at higher altitudes.

4.2. Spatial Variability

[31] The uncertainty due to the sampling error, which is dominated by turbulent eddies, is an atmospheric limit on the accuracy of mixed-layer averages over land due to variance in the vertical profile, imposed by turbulence unresolved in transport models. The value from COBRA data, calculated using equation (1), averaged about 0.2 ppm. It is important to note that in general similar uncertainties affect ground based in situ observations over the continent, representing a temporal ensemble conditioned by the same dynamical processes. Time-averaged mixing ratios are affected from eddies passing by, and uncertainties are associated with these averages reflecting the number of these eddies and the variance they give rise to. This information provides useful weights for inversions, with lower weights associated with periods with higher uncertainty in the time-averaged concentration value, e.g., early morning periods when the mixed layer grows rapidly and entrains a few large eddies with different mixing ratios.

[32] To illustrate this phenomenon, we used a typical time period (7 daytime hours during June) of the Harvard Forest CO_2 time series and applied equation (1) (with altitudes replaced by time) to incorporate the effects of temporal correlations in the uncertainties of temporally-averaged concentrations. Significant variability in the sampling error was found for hourly averages, with values ranging from less than 0.05 ppm to more than 0.35 ppm. The mean sampling error was very similar in magnitude as the sampling error for airborne measurements.

[33] High-quality instruments with precision and bias errors that are small compared to the sampling error are required to resolve spatio-temporal variations in mixed-layer averages. The signal would otherwise be limited by instrument errors rather than by unresolved turbulence. This requirement implies that CO_2 sensors should be capable of measurements traceable to world standards to ±0.1 ppm or better, whether on the ground or in an aircraft.

[34] Atmospheric transport models used for inversions typically have horizontal resolution between 200 and 400 km [*Denning et al.*, 1999]. The corresponding representation errors are 1 to 2 ppm (Figure 5), almost an order of magnitude larger than the sampling errors. The representation error would accrue even for a model with appropriate temporal resolution using data without the current practice of filtering out "high-frequency variability" (= signal). For the COBRA data this analysis suggest that only at a grid size of ∼30 km would the analysis be limited by sampling error rather than by representation error, but quite significant improvement should be realized for models with grid cells of 50 or 100 km, for which representation and sampling errors are comparable. Models with coarser resolution cannot distinguish the signal contained in observed
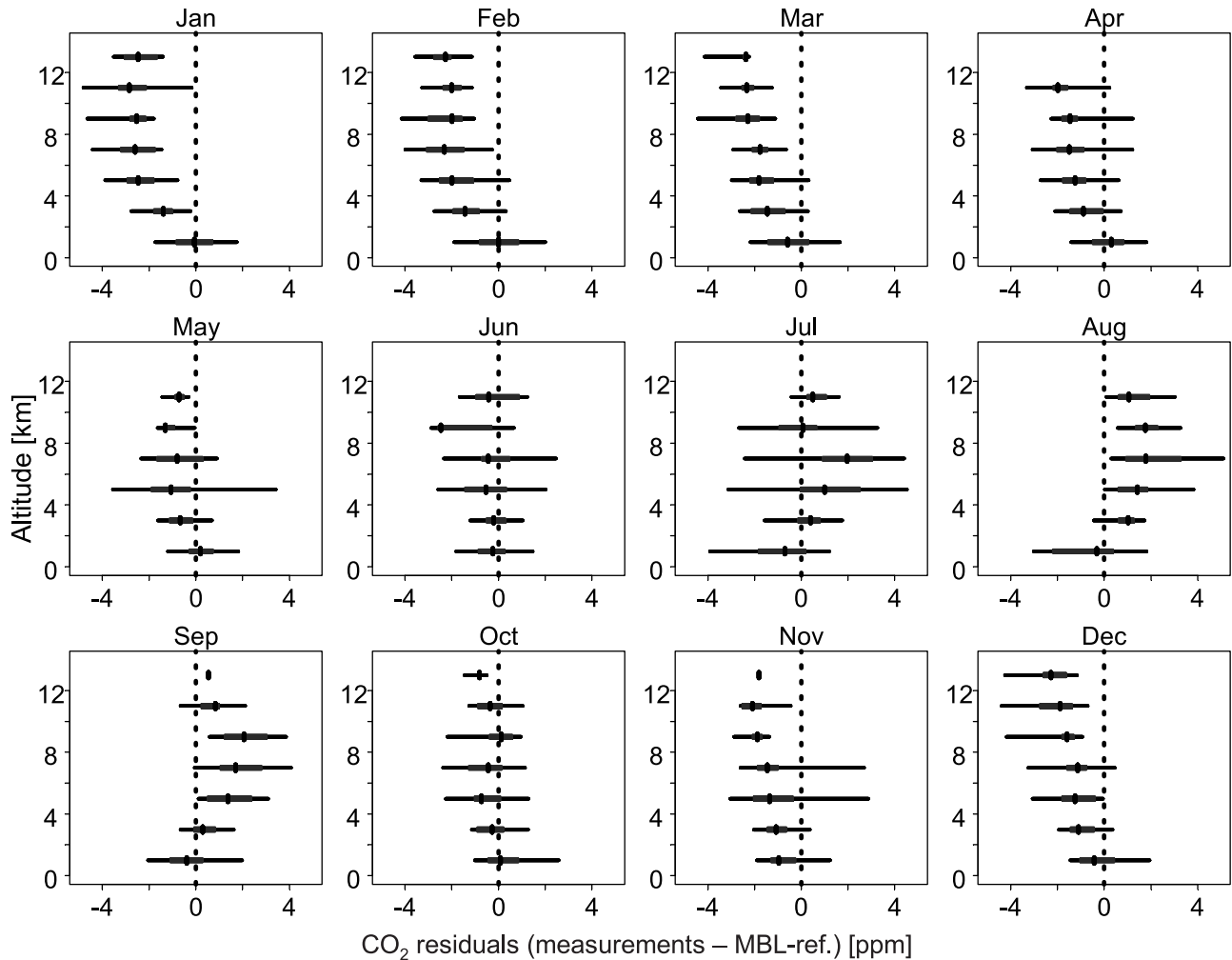
Figure 6. Distribution of residuals between measured CO_2 over the Pacific and MBL-reference CO2 (measurements − MBL-ref.) in ppm (x-axes) for different altitude intervals (y-axes) and for each month. Boxes indicate the central 50%, horizontal lines the central 90%, and vertical bars the median.

spatial variations from uncertainties arising from representation error. Further, the variance associated with representation error is not random. As we show in the companion paper, it is caused by the subgrid variations in surface fluxes affecting a profile. Thus if surface fluxes in the near field environment of a measurement location are not representative for the grid-scale averaged flux, offsets or biases may be expected.

5. Concluding Remarks

[35] We have analyzed COBRA data to characterize the spatio-temporal variance of CO_2 concentrations over North America, and to critically assess the requirements of a model-data fusion system aimed at deriving regional to continental flux estimates from measurements of CO_2 over the continent. The spatial patterns in the CO_2 data collected over the United States during COBRA show clear signatures of terrestrial fluxes during the active growing season. Instruments able to measure CO_2 concentrations to ±0.2 ppm, traceable to world standards, are needed enable measurement of mixed-layer averages from vertical profiles

with an uncertainty solely limited by unresolved turbulence, providing tight constraints for fluxes when used in an appropriate modeling framework.

[36] An assessment of the upstream boundary condition for regional modeling showed that the marine boundary layer reference for CO_2 might introduce significant seasonal biases. If the MBL reference were use without accounting for vertical gradients over the ocean to infer continental sources and sinks, these biases can propagate into artifacts in retrieved fluxes.

[37] A significant fraction of the information in the observed CO_2 signatures over the continent is contained in relatively small spatial and temporal scales. In order to effectively use the information contained in accurate CO_2 measurements, transport models need to resolve these scales; otherwise this fine-scale signal is transformed into large-amplitude unresolved variance (representation error), which can easily be an order of magnitude larger than true atmospheric variance (sampling errors).

[38] A suitable analysis framework that can extract information about surface fluxes from the spatially variable distribution of CO_2, minimizing the representation error
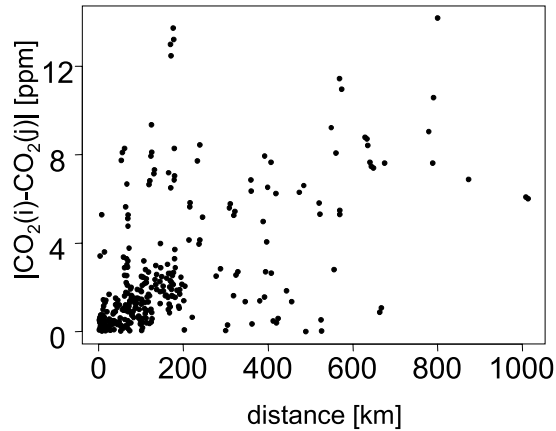
Figure 7. Differences in mixed-layer averaged CO_2 measured at different locations (i, j) within a 3-hour period, plotted against the spatial distance of the measurement locations.

and potential biases, is thus needed. In the companion paper we introduce a modeling framework that tries to address these issues: A transport model is coupled to a data-driven boundary condition with reduced seasonal biases, and to surface fluxes at high spatial and temporal resolution.

Appendix A

A1. Variogram Estimation and Model Fitting

[39] First, a data set of pairs was created containing $S_i - S_j$ and $|x_i - x_j|$, where all possible combinations of two observations where used that were measured within 3 hours of each other, giving 317 different pairs. A plot of $|S_i - S_j|$ versus $|x_i - x_j|$ is shown in Figure 7. The data were grouped by distances into equal sized groups of 30 pairs, with the last group containing 47 pairs. Short horizontal distances usually corresponded to short time differences, basically given by the speed of the aircraft (for example pairs with horizontal distances of about 20 km were on average measured 20 min apart). This ensures better separation of spatial variability from temporal variability. For the pairs in a given group with average distance $|x_i - x_j| = h$ a variogram was estimated using a robust variogram estimator [*Cressie*, 1993]

$$Var(S_i - S_j) = 2\overline{\gamma}(h)$$
$$= \left\{ \frac{1}{N(h)} \sum_{N(h)} |S_i - S_j|^{1/2} \right\}^4 \bigg/ \left(0.457 + \frac{0.494}{N(h)} \right)$$

(A1)

[40] Here $N(h)$ is the number of pairs in the group with distance h; $\overline{\gamma}(h)$ is called the semi-variogram. Variogram estimates $(2\overline{\gamma}(h))$ are shown versus distance h in Figure 8 as filled squares.

[41] In order to allow a spatial simulation of the process, a variogram model has to be fit to the discrete variogram estimates from data, giving a variogram value at any given distance. There are a number of variogram models, for which the main requirement is that they have to be negative

definite (in equivalence to that a covariance must be positive definite) [*Cressie*, 1993]. Out of these different variogram models (Linear, Gaussian, Exponential, Rational quadratic, and Power) the Power-variogram was chosen:

$$2\gamma(h) = 2\left(c_0 + c_1 \cdot h^\lambda\right)$$

(A2)

[42] Here c_0 is the nugget (variance caused by the sampling error $\sigma(\overline{CO_2})$, taken from equation (1)), and c_1 and λ (power) are parameters to be estimated. Since the variogram estimates from equation (A1) are not statistically independent (many distance-groups of pairs share common individual observations), a covariance matrix was estimated using a Jackknife (delete-1) statistics: The variogram estimation was repeated with one observation (mixed-layer average CO_2 and position) deleted at a time (gray symbols in Figure 8), and the variogram error for each distance-group was estimated according to the classical Jackknife statistics [*Cressie*, 1993]. The Power variogram was then fitted using a weighted generalized least square, taking the error covariance into account (solid line in Figure 8). The power variogram fit the data reasonably well, especially in that, for small distances, it exhibits a small slope, avoiding overestimation at small distances typical of many other variogram models. At 150 km and 180 km distance, the fit does not go through the variogram estimates, however, this is caused by the large error for the variogram estimate at these distances, combined with smaller errors at smaller distances. Also, the Power-variogram will fail at larger distances, since the differences between mixed-layer mean signals will not exceed certain values, no matter how far the locations are apart, so one would expect the true variogram to approach some limit on large scales. However, here we
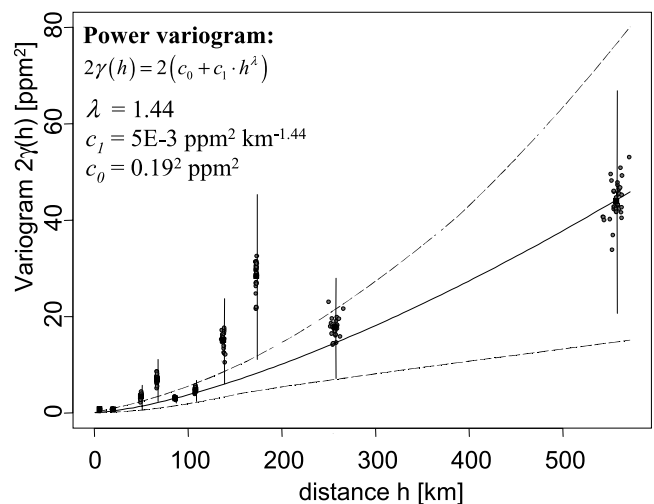
Figure 8. Robust variogram estimates (solid squares) for different distance bins. Points are robust variogram estimates with one observation deleted. Vertical bars represent 1 σ errors derived from the Jackknife delete-1 statistics. The solid line represents a power variogram model fitted to the robust variogram estimates, and the dashed lines correspond to the 95% confidence interval for the variogram fit.
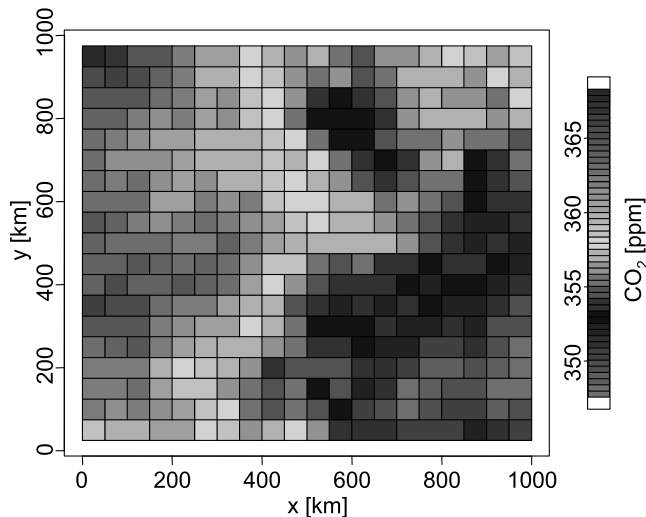
Figure 9. Result of a spatial simulation for a 20 × 20 grid element area. A mean of 365 ppm was assumed, and the spatial variability is determined by the fitted power variogram. See color version of this figure at back of this issue.

are interested in the regional scale, and our approach gives a conservative estimate (lower limit for the variogram).

A2. Spatial Simulation and Representation Error

[43] The spatial simulation was done following *Cressie* [1993]. The simulation was conducted on regular quadratic grids with 20 × 20 = 400 elements for two different grid distances (5 km and 50 km grid size). For each distance (using a 400 × 400 matrix of all possible pairs of grid elements) the variogram was calculated using the fitted Power-variogram, and the covariance was estimated using the following relation:

$$Var(S_i - S_j) = Var(S_i) + Var(S_j) - 2 \cdot Cov(S_i, S_j)$$
$$= 2 \cdot Var(S) - 2 \cdot Cov(S_i, S_j)$$
$$\Rightarrow Cov(S_i, S_j) = Var(S) - Var(S_i - S_j)/2 \qquad (A3)$$

[44] Here the variance $Var(S)$ was assumed to be independent of the location (the following simulation does not depend on this offset in the covariance), such that the covariance is assumed to be only a function of distance. The spatial simulation starts with a field populated by uncorrelated random numbers ε, with unit variance and zero mean. The simulated spatial distribution is then calculated through $\mathbf{S} = \text{mean}(\mathbf{S}) + \mathbf{\Sigma}^{1/2} \cdot \varepsilon$, where $\mathbf{\Sigma}^{1/2}$ is the "square root" of the covariance matrix $\mathbf{\Sigma}$ ($\mathbf{\Sigma}^{1/2} = \mathbf{Q} \, \mathbf{\lambda}^{1/2} \mathbf{Q}'$, with Q the matrix whose columns are the eigenvectors of $\mathbf{\Sigma}$ and with $\mathbf{\lambda}^{1/2}$ as a diagonal matrix with the square roots of the eigenvalues). Figure 9 shows the results of a simulation (one of the ensemble of possible realizations) for the 50 km grid. It is obvious that the variogram determines a certain grain-size for the CO$_2$ distribution, a size over which the concentration does not change more than a given tolerance value.

[45] The representation error depends on the grid size of a transport model, and can be obtained from the spatial simulations (Figure 9) for a given grid size. We calculated the representation error for a model with resolution of, e.g., 200 km as the standard deviation of individual point values within all sub grids of size 200 × 200 km, averaged over 50 simulations. The calculated error (Figure 5) includes both the representation error and the sampling error, since the fitted variogram model included the variance due to the sampling error. The range of possible values for the representation error was estimated by repeating the simulations with extreme parameter values from the variogram (2.5 and 97.5 percentiles).
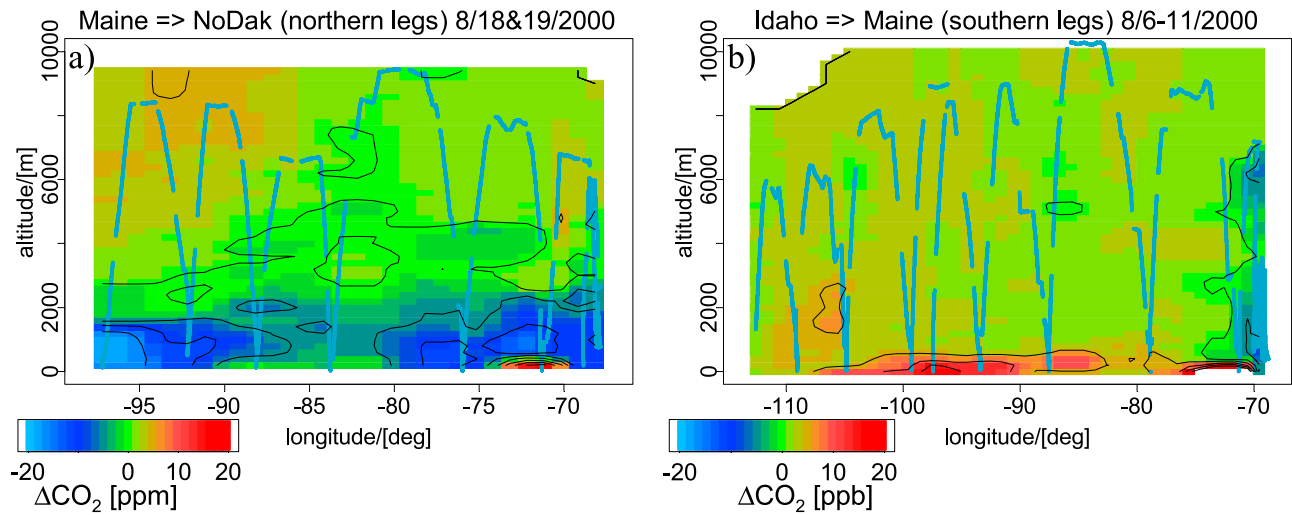
References

Andrews, A. E., K. A. Boering, B. C. Daube, S. C. Wofsy, E. J. Hintsa, E. M. Weinstock, and T. P. Bui, Empirical age spectra for the lower tropical stratosphere from in situ observations of CO$_2$: Implications for stratospheric transport, *J. Geophys. Res.*, *104*(D21), 26,581–26,595, 1999.

Bakwin, P. S., P. P. Tans, C. Zhao, W. I. Ussler, and E. Quesnell, Measurements of carbon dioxide on a very tall tower, *Tellus, Ser. B*, *47*, 535–549, 1995.

Bakwin, P. S., P. P. Tans, D. F. Hurst, and C. Zhao, Measurements of carbon dioxide on very tall towers: Results of the NOAA/CMDL program, *Tellus, Ser. B*, *50*, 401–415, 1998.

Bousquet, P., P. Ciais, P. Peylin, M. Ramonet, and P. Monfray, Inverse modeling of annual atmospheric CO$_2$ sources and sinks: 1. Method and control inversion, *J. Geophys. Res.*, *104*(D21), 26,161–26,178, 1999.

Conway, T. J., P. P. Tans, L. S. Waterman, K. W. Thoning, D. R. Kitzis, K. A. Masarie, and N. Zhang, Evidence for interannual variability of the carbon cycle from the National Oceanic and Atmospheric Administration/Climate Monitoring and Diagnostics Laboratory Global Air Sampling Network, *J. Geophys. Res.*, *99*(D11), 22,831–22,855, 1994.

Cressie, N. A. C., *Statistics for Spatial Data*, John Wiley, Hoboken, N. J., 1993.

Daube, B. C., K. A. Boering, A. E. Andrews, and S. C. Wofsy, A high-precision fast-response airborne CO$_2$ analyzer for in situ sampling from the surface to the middle stratosphere, *J. Atmos. Oceanic Technol.*, *19*, 1532–1543, 2002.

Denning, A. S., D. A. Randall, G. J. Collatz, and P. J. Sellers, Simulations of terrestrial carbon metabolism and atmospheric CO$_2$ in a general circulation model. Part 2: Simulated CO$_2$ concentrations, *Tellus, Ser. B*, *48*, 543–567, 1996.

Denning, A. S., et al., Three-dimensional transport and concentration of SF6: A model intercomparison study (TransCom 2), *Tellus Ser. B*, *51*, 266–297, 1999.

Fan, S., M. Gloor, J. Mahlman, S. Pacala, J. Sarmiento, T. Takahashi, and P. Tans, A large terrestrial carbon sink in North America implied by atmospheric and oceanic carbon dioxide data and models, *Science*, *282*, 442–446, 1998.

Gerbig, C., D. Kley, A. Volz-Thomas, J. Kent, K. Dewey, and D. S. McKenna, Fast response resonance fluorescence CO measurements aboard the C-130: Instrument characterization and measurements made during North Atlantic Regional Experiment 1993, *J. Geophys. Res.*, *101*(D22), 29,229–29,238, 1996.

Gerbig, C., S. Schmitgen, D. Kley, A. Volz-Thomas, K. Dewey, and D. Haaks, An improved fast-response vacuum-UV resonance fluorescence CO instrument, *J. Geophys. Res.*, *104*(D1), 1699–1704, 1999.

Gerbig, C., J. C. Lin, S. C. Wofsy, B. C. Daube, A. E. Andrews, B. B. Stephens, P. S. Bakwin, and C. A. Grainger, Toward constraining regional-scale fluxes of CO$_2$ with atmospheric observations over a continent: 2. Analysis of COBRA data using a receptor-oriented framework, *J. Geophys. Res.*, *108*, doi:10.1029/2003JD003770, in press, 2003.
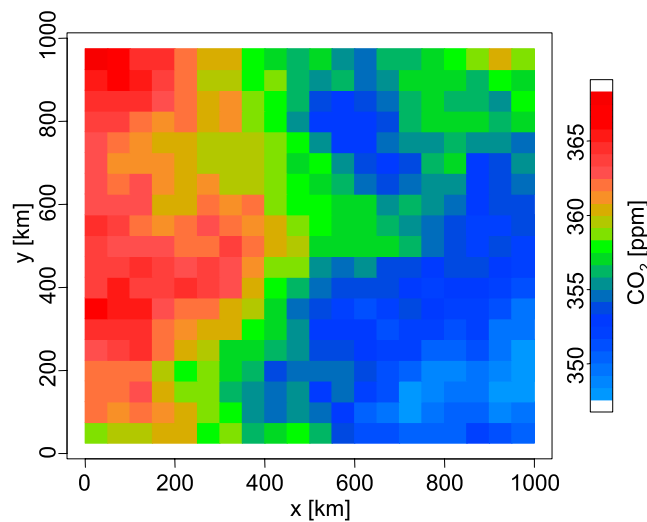
GLOBALVIEW-CO_2, *GLOBALVIEW-CO_2: Cooperative Atmospheric Data Integration Project: Carbon Dioxide* [CD-ROM], NOAA Clim. Monit. and Diagnostics Lab., Boulder, Colo., 2002.

Gloor, M., S. M. Fan, S. Pacala, J. Sarmiento, and M. Ramonet, A model-based evaluation of inversions of atmospheric transport, using annual mean mixing ratios, as a tool to monitor fluxes of nonreactive trace substances like CO_2 on a continental scale, *J. Geophys. Res.*, *104*(D12), 14,245–14,260, 1999.

Gloor, M., S.-M. Fan, S. Pacala, and J. Sarmiento, Optimal sampling of the atmosphere for purpose of inverse modeling: A model study, *Global Biogeochem. Cycles*, *14*(1), 407–428, 2000.

Haszpra, L., Z. Barcza, P. S. Bakwin, B. W. Berger, K. J. Davis, and T. Weidinger, Measuring system for the long-term monitoring of biosphere/atmosphere exchange of carbon dioxide, *J. Geophys. Res.*, *106*(D3), 3057–3069, 2001.

Holloway, J. S., R. O. Jakoubek, D. D. Parrish, C. Gerbig, A. Volz-Thomas, S. Schmitgen, A. Fried, B. Wert, B. Henry, and J. R. Drummond, Airborne intercomparison of vacuum ultraviolet fluorescence and tunable diode laser absorption measurements of tropospheric carbon monoxide, *J. Geophys. Res.*, *105*(D19), 24,251–24,261, 2000.

Kaminski, T., P. J. Rayner, M. Heimann, and I. G. Enting, On aggregation errors in atmospheric transport inversions, *J. Geophys. Res.*, *106*(D5), 4703–4715, 2001.

Kogan, F. N., Global drought watch from space, *Bull. Am. Meteorol. Soc.*, *78*, 621–636, 1997.

Masarie, K. A., and P. P. Tans, Extension and integration of atmospheric carbon dioxide data into a globally consistent measurement record, *J. Geophys. Res.*, *100*(D6), 11,593–11,610, 1995.

Nakazawa, T., K. Miyashita, S. Aoki, and M. Tanaka, Temporal and spatial variations of upper tropospheric and lower stratospheric carbon dioxide, *Tellus, Ser. B*, *43*, 106–117, 1991.

Novelli, P. C., L. P. Steele, and P. P. Tans, Mixing ratios of carbon monoxide in the troposphere, *J. Geophys. Res.*, *97*(D18), 20,731–20,750, 1992.

Sarmiento, J. L., and S. C. Wofsy, A U.S. carbon cycle science plan: Report of the Carbon and Climate Working Group, U.S. Global Change Res. Program, Washington, D. C., 1999.

Stephens, B. B., S. C. Wofsy, R. F. Keeling, P. P. Tans, and M. J. Potosnak, The CO_2 budget and rectification airborne study: strategies for measuring rectifiers and regional fluxes, in *Inverse Methods in Global Biogeochemical Cycles, Geophys. Monogr. Ser.*, vol. 114, edited by P. Kasibhatla et al., pp. 311–324, AGU, Washington, D. C., 2000.

Tans, P. P., I. Y. Fung, and T. Takashi, Observational constraints on the global atmospheric CO_2 budget, *Science*, *247*, 1431–1438, 1990.

Tans, P. P., P. S. Bakwin, and D. W. Guenther, A feasible Global Cycle Observing System: A plan to decipher today's carbon cycle based on observations, *Global Change Biol.*, *2*, 309–318, 1996.

Wei, W. W. S., *Time Series Analysis*, Addison-Wesley-Longman, Reading, Mass., 1989.

Wofsy, S. C., and R. C. Harriss, The North American Carbon Program (NACP), report of the NACP Committee of the U.S. Interagency Carbon Cycle Science Program, U.S. Global Change Res. Program, Washington, D. C., 2002.

Zhao, C. L., P. P. Tans, and K. W. Thoning, A high precision manometric system for absolute calibrations of CO_2 in dry air, *J. Geophys. Res.*, *102*(D5), 5885–5894, 1997.

—————————

A. E. Andrews, NASA Goddard Space Flight Center, Mail Stop 916.0, Greenbelt, MD 20771, USA. (andrews@maia.gsfc.nasa.gov)

C. Gerbig, J. C. Lin, and S. C. Wofsy, Department of Earth and Planetary Sciences, Harvard University, Pierce Hall, 20 Oxford Street, Cambridge, MA 02138, USA. (chg@io.harvard.edu; jcl@io.harvard.edu; steven_wofsy@harvard.edu)

P. S. Bakwin and B. C. Daube, Climate Monitoring and Diagnostic Laboratory, National Oceanic and Atmospheric Administration, R/E/CG1, 325 Broadway, Boulder, CO 80305, USA. (pbakwin@cmdl.noaa.gov; bcd@io.harvard.edu)

C. A. Grainger, Department of Atmospheric Sciences, University of North Dakota, Box 9006, Grand Forks, ND 58202-9006, USA. (grainger@aero.und.edu)

B. B. Stephens, Atmospheric Technology Division, National Center for Atmospheric Research, Boulder, CO 80307, USA. (stephens@ucar.edu)
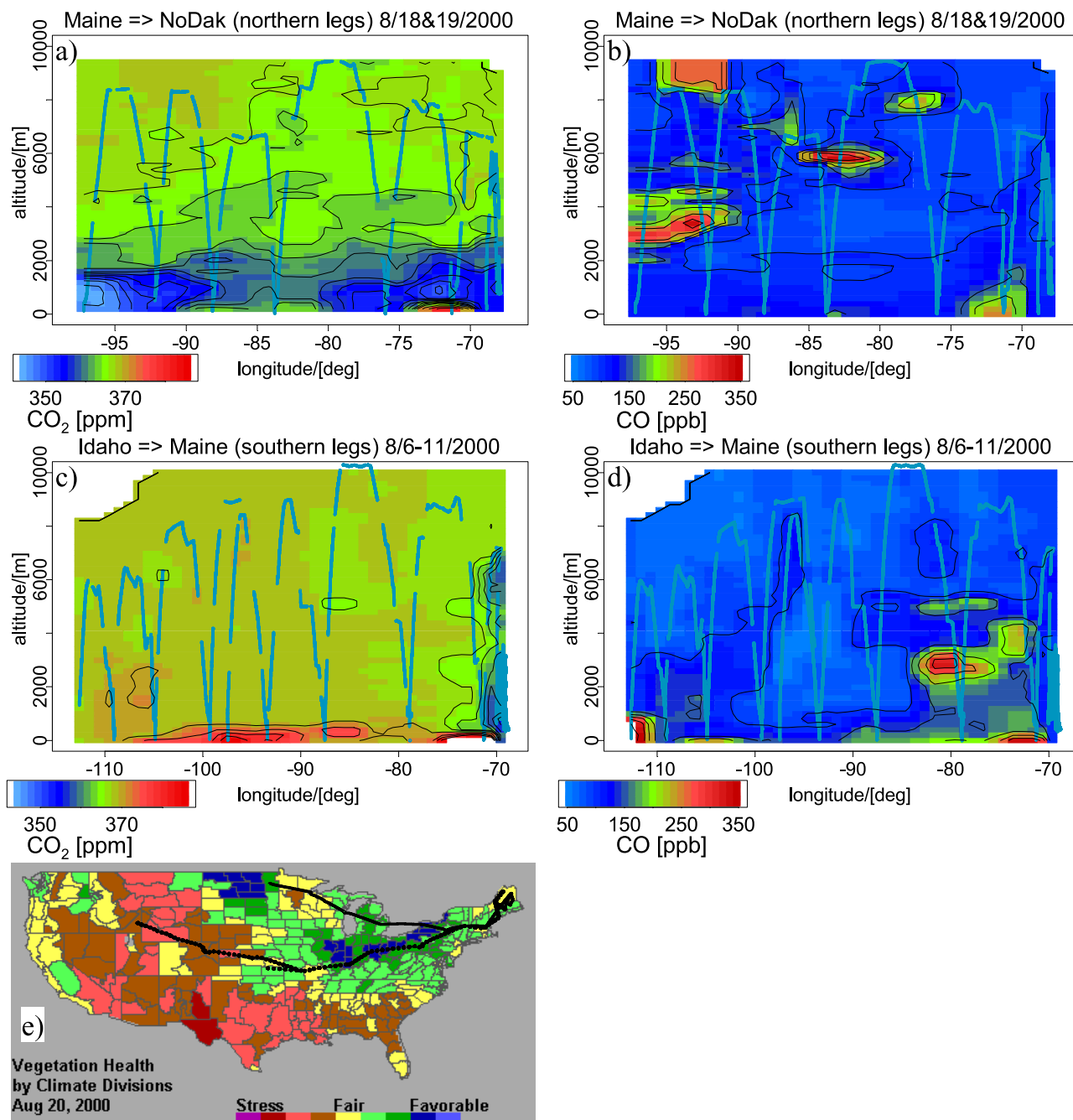
Figure 2. Measured CO_2 and CO distribution as a function of altitude and longitude for the (a and b) northern and (c and d) southern transects, and (e) vegetation condition index (from NESDIS) for 20 August 2000; approximate flight tracks are superimposed. To interpolate the tracer data in altitude and longitude between the measurement locations, the squared inverse of the distance was used as weighting, with the distance measured in units of 500 m vertical and degree longitude horizontal (aspect ratio 1/200). Tracer data from different days and different times of the day are represented in the cross sections (see Table 1).

Figure 3. Difference of measured CO_2 and MBL-reference CO_2 as a function of altitude and longitude for the (a) northern and (b) southern transects. Interpolations are done similar to those in Figure 2.

Figure 9. Result of a spatial simulation for a 20×20 grid element area. A mean of 365 ppm was assumed, and the spatial variability is determined by the fitted power variogram.